Non-Equilibrium Ordering of Liquid Crystalline (LC) Films Driven by External Gradients in Surfactant Concentration

Soumita Maiti 1 , Sangchul Roh 1 , Itai Cohen 2,3 , and Nicholas L. Abbott 1*

- ¹ Smith School of Chemical and Biomolecular Engineering, Cornell University, Ithaca, NY 14853, USA
- ² Laboratory of Atomic and Solid-State Physics, Cornell University, Ithaca, NY 14853, USA
- ³ Kavli Institute at Cornell for Nanoscale Science, Cornell University, Ithaca, NY 14853, USA

E-mail addresses: sm2766@cornell.edu (S. Maiti), sr974@cornell.edu (S. Roh), itai.cohen@cornell.edu (I. Cohen), nla34@cornell.edu (N. L. Abbott)

*Corresponding author at: Smith School of Chemical and Biomolecular Engineering, Cornell University, Ithaca, NY 14853, US. Telephone: (+1) 607-255-3601

Abstract

Hypothesis

Gradients in the concentration of amphiphiles play an important role in many non-equilibrium processes involving complex fluids. Here we explore if non-equilibrium interfacial behaviors of thermotropic (oily) liquid crystals (LCs) can amplify microscopic gradients in surfactant concentration into macroscopic optical signals.

Experiments

We use a milli-fluidic system to generate gradients in aqueous sodium dodecyl sulfate (SDS) concentration and optically quantify the dynamic ordering of micrometer-thick nematic LC films that contact the gradients.

Findings

We find that the reordering of the LCs is dominated by interfacial shearing by Marangoni flows, thus providing simple methods for rapid mapping of interfacial velocities from a single optical image and investigating the effects of confinement of surfactant-driven interfacial flows. Additionally, we establish that surface advection and surfactant desorption are the two key processes that regulate the interfacial flows, revealing that the dynamic response of the LC can provide rapid and potentially high throughput approaches to measurement of non-equilibrium interfacial properties of amphiphiles. We also observe flow-induced assemblies of microparticles to form at the LC interface, hinting at new non-equilibrium approaches to microparticle assembly. We conclude that dynamic states adopted by LCs in the presence of surfactant concentration gradients provide new opportunities for engineering complex fluids beyond equilibrium.

Keywords:

Liquid crystals
Surfactants
Interfacial (Marangoni) flows
Optical mapping

1. Introduction

Gradients in the concentration of surfactants in bulk solution underlie a range of interfacial phenomena because they generate interfacial stresses that trigger advection^{1–6}. The resulting interfacial flows, known as Marangoni flows, give rise to physicochemical processes such as the self-propelled motion of drops^{7–9}, fingering instabilities in thin liquid films^{10–16}, the generation of non-spherical emulsion drops¹⁷ or the appearance of flow patterns inside droplets that suppress the "coffee-ring effect" ^{18,19}. In each of these contexts, understanding the interfacial gradients in surfactant concentration and associated interfacial flows is fundamental to describing the phenomenon.

Past approaches to experimental measurement of interfacial flows driven by surfactant concentration $gradients^{4,20-24}$ include the tracking of fluorescently tagged surfactants^{4,21,22} or microparticles^{20,25}. While important insights have emerged from these approaches, the need for fluorescent tags limits the range of surfactants that can be studied²² and microparticle tracking requires the tracking of multiple microparticles over a series of time points to construct a velocity field²⁵. In this paper, we report observations of dynamic ordering transitions in thermotropic liquid crystal (LC) thin films that occur in the presence of surfactant concentration gradients. When viewed through crossed polars, the LCs generate two-dimensional optical maps arising from interfacial flows regulated by an interplay of transport and interfacial kinetic properties of the surfactants. We conclude that nematic LCs provide new ways to rapidly explore and understand surfactant-driven interfacial flows, including flows that arise from microscopic gradients in surfactant concentration.

A number of past studies by us and others have reported that nematic LCs can be used to optically report equilibrium as well as non-equilibrium interfacial events^{26–28}. Because LC phases possess long-range orientational order, which gives rise to anisotropy in optical and elastic properties, they offer the capacity to amplify and optically report the presence of a range of interfacial species that perturb

LC ordering^{29–35}, including aqueous soluble surfactants^{36–41}. In particular, studies of the reversible adsorption of surfactants at aqueous-thermotropic (oily) LC interfaces have established that the orientations of LCs change as surfactant monolayers interact with the LCs (e.g., via interdigitation of the surfactant tails with the mesogens forming the LC)^{36,37}, hinting at the potential utility of LCs to optically report the presence of gradients in surfactant concentration at interfaces.

Our exploration of the reordering of LCs in the presence of surfactant concentration gradients was additionally motivated by the knowledge that interfacial flows can drive changes in the orientations of thin films of LCs^{26–28}. For example, a recent study revealed that fusion of a single phospholipid vesicle at the aqueous-LC interface can generate transient Marangoni flows that shear-align the LC and generate bright optical flashes ('blinking') of the LC when viewed through crossed polars²⁶. Furthermore, it has been reported that flow of an aqueous surfactant solution (with a uniform bulk concentration) past a LC interface can drive reorganization of the surfactant on the interface in ways that are reflected in the ordering and optical appearance LCs²⁷. However, the ordering of LCs in the presence of imposed, bulk solution surfactant concentration gradients has not previously been explored.

Our study reports four key advances related to the influence of surfactant concentration gradients on LC ordering. First, we show that micrometer-thick nematic LCs films, when exposed to gradients in surfactant concentration generated via use of millifluidic channels, assume non-equilibrium states that reflect the magnitudes of the gradients. Second, we resolve whether the response of the LC is dominated by spatial variations of the LC interfacial surfactant concentration (giving rise to position-dependent anchoring of the LC) or shear-induced ordering of the LC arising from interfacial flows. Third, we elucidate the key interfacial transport and kinetics processes that regulate the reordering of the LCs. Finally, we determine the effects of confinement on surfactantdriven interfacial flows and the non-equilibrium ordering of LC, and thereby provide insights into the design of LC domains that have tailored responses to surfactants and their concentration gradients.

We end this Introduction by placing our study into one additional context, namely natural and technological principles for measuring solute concentration gradients. Specifically, in contrast to the approach described in this paper, in both natural and engineered systems, gradients in the concentration of chemical species in solution are typically not measured directly, but rather characterized by measuring two or more point concentrations^{42–56}. The gradient is inferred by comparing the two-point concentrations, as determined at different times or positions⁴²⁻⁴⁶. Although concentration gradients can be detected by using the deflection of a laser beam transmitted through a solution^{57–60}, the technique does not scale to microscopic gradients. We envisage that LC-based methods for characterizing concentration gradients (magnitude and direction) of surface-active solutes might find use as microscopic sensors e.g., for guiding chemotaxis of microrobots^{61,62}.

2. Materials and methods

2.1 Materials

4-cyano-4'-pentylbiphenyl (5CB) was purchased from HCCH (Jiangsu Hecheng Display Technology Co., Ltd.). Sodium dodecyl sulfate (SDS, ≥ 99.0% purity) and sodium chloride (NaCl, ≥ 99.5% purity) were purchased from Sigma-Aldrich. Polyimide (PI; SE5661) was purchased from Nissan Chemical Industries, Ltd. The photoresist SU-8 was purchased from Kayaku Advanced Materials. All chemicals were used as received without purification. Glass slides (Fisher Finest Premium grade) and hexanes were purchased from Fisher Scientific. Octadecyltrichlorosilane (OTS) was purchased from Sigma-Aldrich. Silica (diameter of 3 μm) and polystyrene (diameter of 2 μm) microparticles were purchased from Cospheric and Thermo Fisher Scientific, respectively. Acrylic sheets (thickness of 1.6 mm) were purchased from ZLazr.. Transmission electron microscopy (TEM) grids were purchased from Electron Microscopy Sciences. Purification of water (18.2 M Ω cm resistivity at 25°C) was performed using a Milli-Q water system.

2.2 Preparation of polyimide-coated glass substrates

Glass microscope slides were cleaned with Alconox cleaning formulation followed by rinsing with deionized water and ethanol. Next, the slides were incubated in Nochromix solution (a mixture of Nochromix and 98% sulfuric acid) for 1 day. The slides were thoroughly rinsed five times with 100 mL of deionized water and then dried under a stream of

gaseous N_2 . Clean glass surfaces were then coated with polyimide solution (by spin coating) and baked at 80 $^{\circ}$ C for 10 minutes followed by 210 $^{\circ}$ C for 1 hour. The PI used in our study caused perpendicular (homeotropic) anchoring of the LC.

2.3 Preparation of LC films

Thin films of 5CB were prepared by pipetting 0.3 μL of 5CB into the pores of TEM grids (thickness of 18 $\mu m)$ supported on PI-coated glass microscope slides. The excess LC was removed using a capillary tube.

2.4 Generation of surfactant concentration gradients using milli-fluidic channels

Milli-fluidic channels with a rectangular cross-section (40mm x 5mm x 1.6mm), as shown in Fig. 1d, were fabricated by laser cutting of acrylic plastic sheet (thickness of 1.6 mm). The bottom of the channel was prepared from a treated glass microscope slide. The glass microscope slide was coated with PI (as described above) and then used to support a TEM grid that was filled with LC. The bottom glass substrate was attached to acrylic channel using binder clips. Two identical syringes (20 ml, Henke-Sass Wolf, Germany) were filled with aqueous solutions of SDS at different concentrations and attached to the two inlets of the channel. The solutions were delivered by a syringe pump (KD Scientific) at equal flow rates unless mentioned otherwise. All the aqueous solutions contained 300 mM NaCl.

2.5 Preparation of microwells on glass substrates

To prepare LC domains with lateral sizes that differed from the TEM grid slots, we patterned SU-8 on clean glass surfaces to create microwells with dimensions of 400 $\mu m \times 200 \ \mu m \times 20 \ \mu m$. The microwells were pretreated with OTS (1 % vol/vol in hexanes; 30 mins) and then rinsed with chloroform and water, to cause perpendicular anchoring of LC. The microwells were filled with LC and used in studies of the formation and localization of microparticles at the LC interface (see Fig. 8 below).

2.6 Microscopy observations

An Olympus BX41 microscope with 4X and 10X objectives, two rotating polarizers, and a Moticam 10.0 MP camera was used for optical microscopy.

2.7 Measurements of optical retardance of LC films

Optical retardance of the LC films was measured by comparing interference colors generated under white-light illumination with a calibration chart. Preparation of the calibration chart is described elsewhere²⁷.

3. Results and discussion

3.1 Optical response of LC to gradients in bulk concentration of surfactant

Our initial goal was to determine if thin films of nematic LCs (5CB; Fig. 1a) would undergo ordering transitions when contacted by aqueous solutions containing gradients in surfactant concentration (sodium dodecyl sulfate (SDS; Fig. 1b)). We prepared thin films of LC by hosting 5CB in the pores of copper grids (slot area 285 µm x 285 µm and thickness 18 µm) supported on polyimide (PI)-coated glass microscope slides (Fig. 1c), as described in the Materials and Methods section. The PI coating was selected to cause a perpendicular (homeotropic) orientation of the LC at the PI-LC interface. When incubated under an aqueous solution containing at least 0.016 mM SDS in 300 mM NaCl (NaCl was added to avoid the formation of aqueous droplets at the LC-solid interface, as reported in a previous study⁶³ and it is added to aqueous solutions at a concentration of 300 mM in all the experiments described below), the LC films exhibited a appearance (Fig. 1c) consistent perpendicular anchoring of 5CB at the aqueous-LC interface.

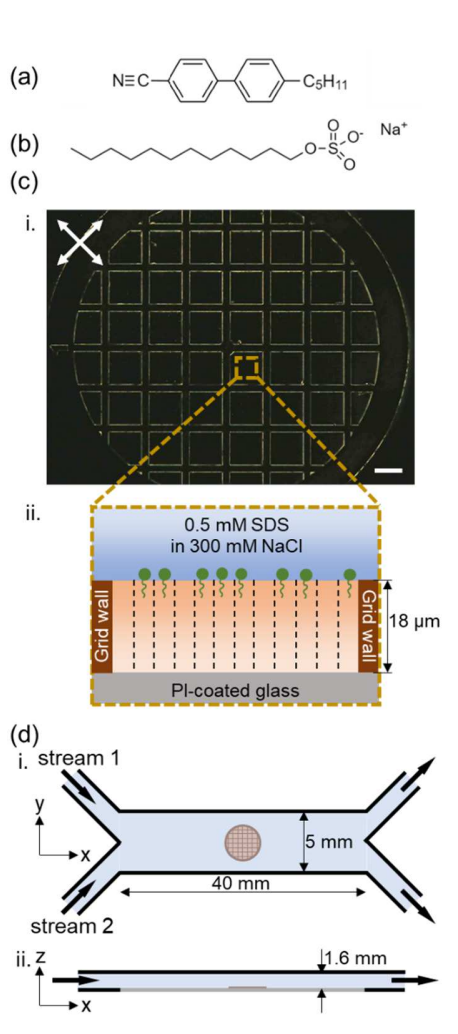


Fig. 1. Molecular structure of (a) 4-cyano-4'-pentylbiphenyl (5CB) and (b) sodium dodecyl sulfate (SDS). (c) A film of LC supported on a PI-coated glass is immersed in the aqueous solution of 0.5 mM SDS in 300 mM NaCl solution. (i) Optical micrograph of the LC film between crossed polars at the equilibrium state. The scale bar is 250 μ m. (ii) Schematic illustration of the LC director profile across the thickness of the film. (d) Schematic of the milli-fluidic channel used to generate gradients in concentration in bulk solutions (i) top view, (ii) side view.

To characterize the LC response to gradients in SDS concentration, we attached the PI-coated glass substrate supporting the LC film to the floor of a millifluidic channel (Fig. 1d; detailed elsewhere²⁷). The gradient in SDS concentration was generated within the milli-fluidic channel by pumping two aqueous solutions containing different concentrations of SDS through the channel inlets under conditions of laminar flow (Fig. 2e).

We confirmed that the flow of the bulk aqueous phase through the milli-fluidic channel did not cause a realignment of the LC via flow-induced interfacial shear stresses²⁷ by pumping two solutions (each at 2 mL/min) with the same SDS concentrations (either 0.25 mM SDS or 0.5 mM SDS) through both inlets of the channel. The dark optical appearance of the LC film (Fig. 2a-d) in the presence of the flowing SDS solution indicates that the orientation of the LC remained perpendicular to the LC-aqueous interface. We calculated the Reynolds number, Re, as Re = $d_h^*v^*\rho/\mu$, where d_h is the hydraulic diameter of the channel, v is the linear velocity of the aqueous solution, ρ is density and μ is viscosity of the SDS solution (see SI for details). Since the calculated Re was 39, the flow inside the channel will be laminar, as needed to generate well-defined surfactant concentration gradients in the following experiments.

The diffusion length over which the gradient in surfactant concentration is formed at the interface between the two aqueous SDS streams entering the channel (hereafter called the 'width of the bulk solution concentration gradient'; see inset in Fig. 2e) evolves with position down the channel (defined as xdirection) due to the increasing time of contact between the two streams. In the experiments described below, we placed the LC film 20 mm downstream from the channel entrance and we pumped two aqueous solutions containing 0.25 mM SDS and 0.5 mM SDS at 2 mL/min into each inlet of the milli-fluidic channel flow (Fig. 2e;). Under these conditions, we calculate the width Δy of the bulk solution SDS concentration gradient as $\Delta y = (2*D*t)^{1/2}$, where D = $5.7x10^{-10}$ m²/s is the self-diffusion coefficient of SDS^{64} and t = x/v = 1.39 s is the time of contact of the two streams and x = 0.02 m is the downstream position of the LC film from the channel entrance. This leads us to estimate Δy to be 40 μm in our initial experiments.

When using the experimental conditions described above, Fig. 2f reveals that we observed the LC film to exhibit (between crossed polars oriented at 45° to the bulk flow direction) a bright optical band that spanned the LC film in the downstream direction. The dark optical appearance of the LC on either side of the bright band is consistent with the presence of a perpendicular orientation of the LC induced by SDS solutions with uniform concentrations (0.25 mM or 0.5 mM; see Fig. 2a-2d). By varying the flow rates of the inlet streams independently of each other, we observed the position of the bright LC band to change in a manner that tracked the predicted location of the

interface between the two inlet streams (Fig. S2 and Video S2). Additionally, within each square domain of the grid that hosted a bright domain of LC, a progression of interference colors was observed along a direction (y-direction) orthogonal to the bulk flow direction. The observed progression of interference colors evident in Fig. 2f (quantified below as optical retardance) indicates that the LC film assumes a range of tilted states. Overall, these observations provide the first evidence that the presence of a gradient in surfactant concentration in the bulk aqueous solution generates a change in ordering of the LC and associated optical response. Interestingly, however, inspection of Fig. 2f reveals that the width of the bright optical band (\sim 285 µm) is defined by the width of the LC domains (285 μ m), whereas the predicted width (see above) of the bulk SDS concentration gradient is much smaller (\sim 40 μ m). These observations are addressed in the sections that follow.

3.2 Influence of the magnitude of the surfactant concentration gradient on LC optical response

We varied the magnitude of the surfactant concentration gradient, G, defined as $\Delta C/\Delta y$, where ΔC is the difference in surfactant concentration between the two inlet streams and Δy denotes the width of the bulk concentration gradient, by either changing ΔC (using inlet streams with different surfactant concentrations) or by altering Δy (by varying the flowrates of the streams). Initially, we varied ΔC from 0.1 mM to 0.25 mM using the following pairs of aqueous SDS solutions: (0.5 mM and 0.4 mM), (0.4 mM and 0.25 mM) and (0.5 mM and 0.25 mM). During these experiments, the flow rates of the inlet streams were held constant (rows in Fig. 3a). For example, by moving from left to right along the middle row of Fig. 3a, pairs of aqueous streams with distinct concentrations are pumped at a constant overall flow rate of 4 mL/min through the channel (corresponding to $\Delta y = 40 \mu m$), thus generating bulk gradients in surfactant concentration with magnitudes of 2.5 mM/mm, 3.8 mM/mm and 6.3 mM/mm, respectively. In our second approach, we varied the flow rates of both aqueous streams (at 0.1 mL/min, 2 mL/min, or 5 mL/min) thus varying Δy while keeping ΔC constant (columns in Fig. 3a). We calculated Δy to be 178 μm , 40 µm or 25 µm for overall flow rates, Q, of 0.2 mL/min, 4 mL/min, or 10 mL/min, respectively. Accordingly, by decreasing Q at constant $\Delta C = 0.15$ mM (top to bottom along the middle column in Fig. 3a), G was calculated to decrease from 6.0 mM/mm to 0.8 mM/mm (through 3.8 mM/mm).

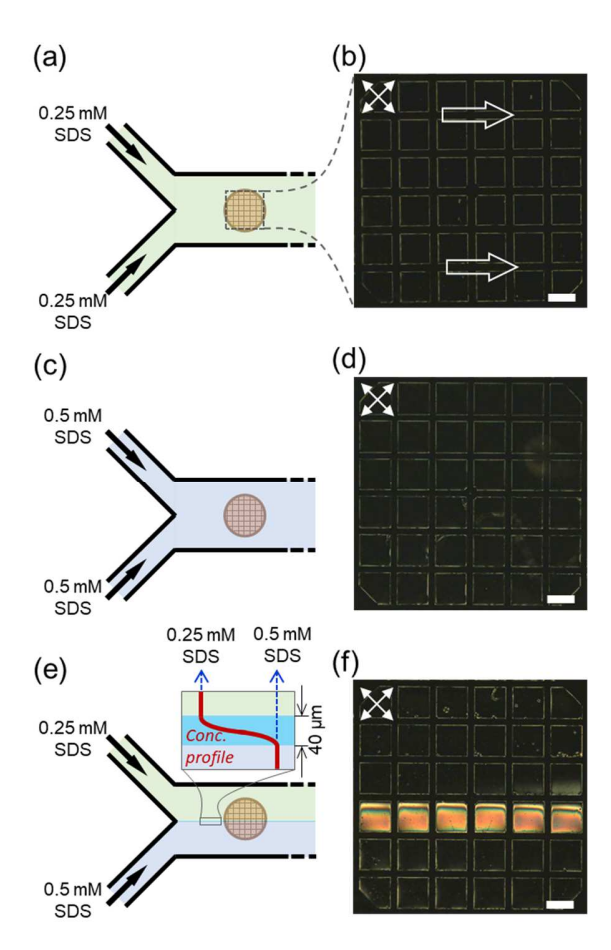


Fig. 2. (a-b) Aqueous solution of 0.25 mM SDS is pumped through both the inlets of the channel at a flow rate of 2 mL/min each. (a) Schematic illustration of the flow condition; (b) Optical response of the LC film between cross polars. Arrows indicate the direction of the bulk flow; (c-d) Aqueous solution of 0.5 mM SDS is pumped through both the inlets of the channel at a flow rate of 2 mL/min each. (c) Schematic illustration of the flow condition; (d) Optical response of the LC film between cross polars; (e-f) Aqueous solutions of SDS at 0.25 mM and 0.5 mM concentrations (color-coded as green and blue, respectively) are passed through two inlets of the channel at a flow rate of 2 mL/min each to define a gradient in SDS concentration in the bulk aqueous solution. (e) Schematic illustration of the flow condition. The concentration profile of SDS near the middle of the channel width is illustrated in the inset; (f) Optical response of the LC film to the gradient in SDS concentration. Scale bars are 250 μm .

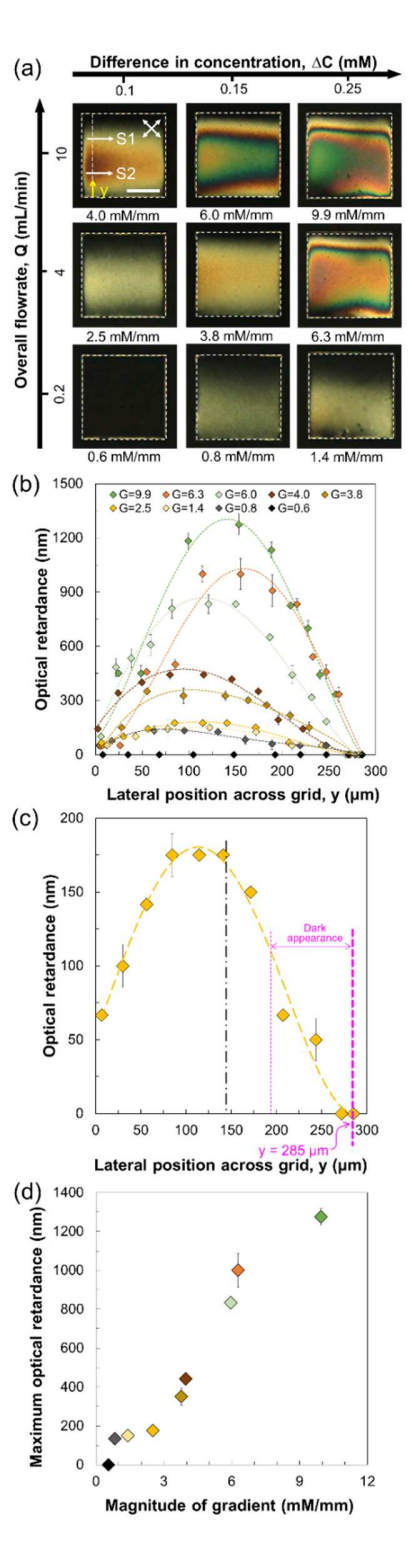


Fig. 3. Influence of the magnitude of the surfactant concentration gradient in the bulk solution on the optical response of the LC: (a) Difference in surfactant concentration between the two inlet streams (along horizontal) and the overall flow rate of the inlet streams (along vertical) are varied to change the magnitude of the

external gradient. The optical response of LC between crossed polars is shown for each condition. The calculated value of G corresponding to each gradient condition is reported below the LC optical response. The horizontal arrows on the optical response in the first cell represent the direction of bulk flow of the aqueous solutions where the stream with higher SDS concentration is in the lower half of the image. The scale bar is $100 \mu m$. (b) The optical retardance of the LC films is plotted against the lateral position across the square grids for different magnitudes (unit: mM/mm) of the gradient. Optical retardance is measured along the dotted line shown on the optical response in the first cell of (a), which is similar for each of the conditions. (c) The optical retardance of the LC film in response to a gradient in SDS concentration of magnitude G = 2.5 mM/mm, plotted against the lateral position across the square grid. The dashed vertical line indicates the centerline of the LC film. The grid walls are located at y = 0 and $y = 285 \mu m$ (dashed pink line on the extreme right). Error bar: S.D. with n = 3. (d) A plot of maximum optical retardance versus magnitude of the imposed gradient of SDS in bulk solution. Error bar: S.D. with n = 3.

The matrix of LC optical responses in Fig. 3a reveals a qualitatively similar progression of LC interference colors in the y-direction (direction of predicted SDS gradient) across each sample, independent of the magnitude of the surfactant concentration gradient. The interference color within each LC domain that corresponds to the highest value of optical retardance is located towards the middle region of the grid (e.g., for G = 6.3 mM/mm, the orange band in the middle corresponds to an optical retardance of 1000 ± 86 nm; see Materials and Methods), a result that is consistent with our observation in Fig. 2f. When the gradient is increased by increasing ΔC (left to right across the rows), there is an increase in the number of interference bands (in the y-direction) evident across each LC domain. This result indicates that the maximum optical retardance exhibited by the LC increases with the magnitude of the surfactant concentration gradient. Similarly, by moving upward along the columns of images in Fig. 3a, the surfactant concentration gradients increase in magnitude due to a decrease in Δy . Here also we observe that the maximum value of the LC optical response (optical retardance) to increase with the magnitude of the gradient. Finally, we point out the asymmetry in the optical response of the LC relative to the centerline of the LC domain. For example, optically dark regions are observed near the top edges of the LC domains (but not bottom edges) in all images in Fig. 3a. The dark regions are particularly pronounced for weak SDS gradients (for values of G < 4.0 mM/mm). The optically dark regions, which will be discussed in later sections

of this paper, are caused by LC alignment along the interface-normal due to surfactant-induced immobilization of the interface²⁷.

We quantified the optical responses evident in Fig. 3a by measuring the optical retardance of the LC films along the y-direction (see dotted line in Fig. 3a) (Fig. 3b). Inspection of Fig. 3b reveals that each sample exhibited a maximum in optical retardance towards the center of the LC domain (in the y-direction). Although the position of the peak in Fig. 3b was determined to be influenced by the location of the gradient relative to the LC grid between samples (see Fig. S1), we generally observed the LC optical retardance to exhibit an asymmetric variation with respect to the centerline of the grid (Fig. 3c shows an example where the asymmetry is clearly evident). The value of the maximum in optical retardance is a quantity that we found to correlate strongly with the magnitude of the bulk surfactant concentration gradient (Fig. 3d). Overall, the results in Fig. 3 provide support for our conclusion that the LC films undergo ordering transitions in response to surfactant concentration gradients and that the magnitude of the gradient impacts the optical response.

3.3 The role of Marangoni flows

To explore further the origins of the dynamic reordering of the LC films shown in Fig. 2 and Fig. 3, we investigated the LC response to gradients in the concentration of surface-inactive solutes in bulk solution. We sought to determine if osmotic flows induced by concentration differences would trigger a LC response⁶⁵⁻⁶⁷. First, we investigated gradients in the concentration of methyl blue (MB), a surfaceinactive dye (see SI for detail), as its optical absorbance enabled us to optically characterize concentration gradients in bulk solution (Fig. 4b, 4e). To generate a gradient in the concentration of MB, we used two aqueous streams containing the same SDS concentration of 0.5 mM with MB (0.37 mM) added to only one of the two inlet streams (Fig. 4a). The optical image (obtained with a single polarizer in the optical path) presented in Fig. 4b confirms the presence of a gradient in the concentration of MB. However, the LC film in contact with the MB concentration gradient, when viewed between crossed polarizers, was uniformly dark (Fig. 4c). This result indicates that a gradient in MB concentration does not perturb the initial homeotropic orientation of the LC (e.g., via an osmotically-driven flow). Thus, bulk concentration gradients of solutes do not directly lead to the LC optical responses shown in Fig. 2 and Fig. 3. However, when gradients in SDS and MB concentrations were generated in solution (Fig. 4d-f), we observed the LC optical response to coincide with the MB gradient. The maximum optical retardance of the LC was $\Delta r = 1000 \pm 86$ nm with (Fig. 4f) or without MB (Fig. 2f)), indicating that the presence of MB does not interfere with the response of the LC to the gradient in concentration of SDS. We make an additional observation. While the imposed gradient in SDS concentration generated an LC optical response, we did not observe the MB concentration gradient to be measurably changed by the SDS gradient (see SI).

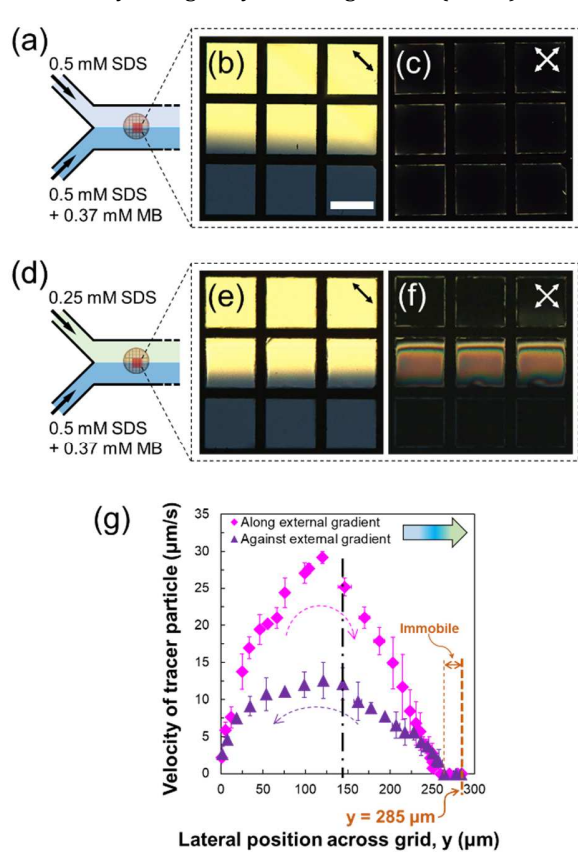


Fig. 4. Effect of surface activity of solutes on LC optical response to concentration gradients in the bulk solution: (a) Two streams of 0.5 mM SDS solution, one containing 0.37 mM MB and the other without MB are pumped through the two inlets of the channel at a flow rate of 2 mL/min each. (b,c) Optical response of LC film under the flow condition described in (a). (b) Optical response of the LC film with single polarizer; (c) Optical response of the LC film between crossed polars; (d) 0.25 mM SDS solution is pumped through one inlet and a solution containing 0.5 mM SDS and 0.37 mM MB is pumped through the other inlet of the channel at a flow rate of 2 mL/min each. (e) Optical response of the LC film with single polarizer; (f) Optical response of the LC film

between crossed polars under the flow condition described in (d). (g) Velocity of circulating tracer particles (covering the entire width of the LC domain) dispersed in LC in presence of a gradient in SDS, condition described in Fig. 2e. The arrow on the top right corner of the plot depicts the direction of the external gradient in SDS concentration. The broken arrows in pink and purple represent the direction of motion of the tracked particles. The broken line in black shows the centerline of the LC film. The grid walls are located at y=0 and $y=285~\mu m$ (broken lines in orange on the extreme right). Error bar: S.D. with n=3. The scale bar is 250 μm and is the same for all the optical images.

The results above, when combined, lead us to propose that the LC optical response to the SDS concentration gradient arises from a gradient in the concentration of SDS at the aqueous-LC interface. As described in prior studies^{1,68}, interfacial surfactant concentration gradients arising from the presence of bulk concentration gradients are governed by an interplay of five transport processes, namely, diffusion of surfactant from the aqueous phase across a nearsurface boundary layer, adsorption of surfactant at the aqueous-LC interface, diffusion and advection of surfactant along the aqueous-LC interface, and desorption of surfactant from the aqueous-LC interface into the bulk aqueous phase (Fig. 5a). We propose that a gradient in interfacial surfactant concentration generated via these processes exerts two potential influences on the LC. First, it generates a gradient in surface pressure of SDS that drives a net interfacial flow (Marangoni flow) in the direction of decreasing surface concentration of SDS (along the v-direction from higher surface pressure to lower surface pressure). This interfacial flow generates a circulating flow within the LC film (to conserve the LC mass due to confinement of the LC domains by the grid walls) that results in shearing of the LC. The shearing of the LC drives a reorientation of the LC away from the surface normal and thus generates a bright optical response. Second, the presence of a gradient in surface concentration of SDS can lead to a position-dependent anchoring (orientation or anchoring energy)⁶⁹ of the LC at the interface due to changes in the interactions of the LC and the local surfactant concentration across the interface (see Introduction). Below we first explore the influence of Marangoni flows on the LC, and then demonstrate that the effects associated with positiondependent anchoring of the LC across the interface are small compared to the Marangoni flows.

To provide initial support for the above-proposed role of Marangoni flows on the LC response, we dispersed

silica particles (3 µm in diameter) in the film of LC and observed the silica particles to exhibit a steady circulatory motion inside the LC film (Video S1). As described in prior studies of surface-driven circulatory flows within cavities, 70,71 tracer particles that explore the entire width of the LC domain pass close to the aqueous-LC interface during their circulation and thus report the interfacial velocity. As detailed below in the context of comparisons of experiments and model predictions of interfacial velocities, we measured the velocities of isolated tracer particles near the aqueous-LC interface to vary with position across the interface (see SI for details) and magnitude of the applied surfactant concentration gradient. Specifically, the tracer particle velocity exhibited a maximum close to the middle of the LC domain (Fig. 4g), which correlates closely to the location of the maximum in optical retardance of the LC reported in Fig. 3b. Additionally, an asymmetry in the spatial variation of surface velocity is evident in Fig. 4g, similar to that observed with the LC optical retardance presented in Fig. 3c (details in Fig. S4). Below we discuss the key physical processes that connect the concentration gradients of SDS in bulk solution to aqueous-LC interfacial advection and LC optical response.

3.4 Interfacial surfactant coverage and interfacial velocity

To simplify our analysis, we considered the aqueous-LC interface to be divided into two regions (Fig. 5a): the first region (Region 1) contacts aqueous solution containing the high concentration of SDS, and the second region (Region 2) contacts the aqueous solution containing the gradient in bulk SDS concentration as well as the region with the low concentration of SDS. Below we discuss these regions in sequence.

Region 1: The dominant physical process occurring in Region 1 is the adsorption of SDS from bulk solution onto the LC-aqueous interface, and lateral transport of the adsorbed SDS towards Region 2 of the interface. To determine if the surfactant adsorption process is diffusion-controlled or kinetically-controlled, we calculated a Damkohler Number, Da, defined as the ratio of the diffusion time to the adsorption time. The diffusion time is evaluated as $(\Gamma/C_B)^2/D$, where $\Gamma = \Gamma_{eq1}$ is the surface concentration of SDS in equilibrium with a bulk SDS solution of concentration $C_B = 0.5$ mM (estimated to be 4.43 x 10^{-6} mol/m² using the Gibbs adsorption isotherm; see SI for details), and D is the diffusion coefficient of SDS in aqueous 300 mM NaCl $(5.7 \times 10^{-10} \text{ m}^2/\text{s})^{64}$. The adsorption time is expressed

as Γ/k_aC_B , where k_a is the adsorption rate constant of SDS (20 m/s)⁷². Since the calculated value of Da (3 x 10⁵) is much greater than unity, we conclude that the SDS adsorption process is diffusion-controlled⁷³.

Next, we determined if Region 1 possesses a gradient in surface concentration, which would arise if the time required for diffusion-controlled adsorption is comparable to the time for transport of surfactant across the interface to Region 2. Because Da >> 1 (see above), the adsorption length across the LC interface in Region 1 (la; shown in Fig. 5b) can be expressed as la ~ $v_s(\Gamma/C_B)^2/D$, where v_s is the measured interfacial velocity. Using v_s = 30 $\mu m/s$, the maximum interfacial velocity measured using silica tracer particles near the aqueous-LC interface (see Fig. 4g), we calculate that la \sim 4 x 10^{-6} m, which is very small compared to the width of Region 1 (140 x 10⁻⁶ m). This comparison leads us to conclude that the interfacial concentration of surfactant on the upstream section of the LC interface (Region 1) will be effectively uniform, as shown in Fig. 5b.

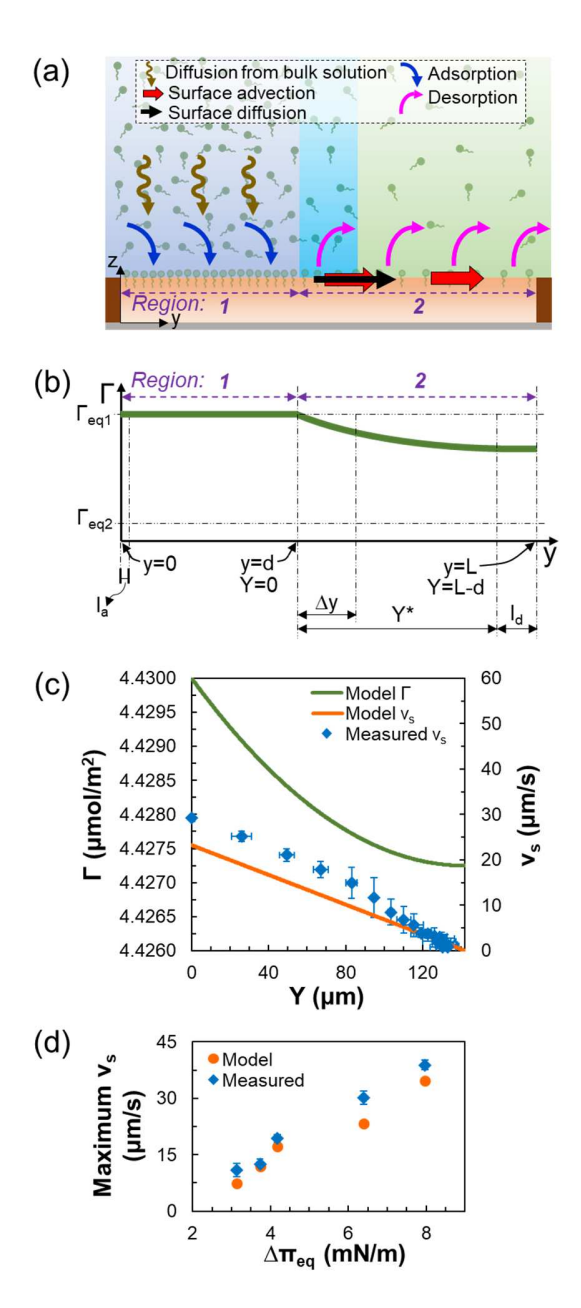


Fig. 5. (a) Schematic of the cross-sectional view (y-z plane) of the experimental system illustrating five transport processes (diffusion of surfactant across the subsurface layer, adsorption of surfactant, desorption of surfactant, surface advection, and surface diffusion of surfactant) associated with the establishment of the surface concentration gradient. The aqueous-LC interface is divided into two sections: Region 1 and Region 2. (b) Schematic illustration of the distribution of surface concentration of SDS across the entire interface (Region 1 and Region 2). The y axis in Region 2 has been redefined as Y with the origin (Y = 0) shifted to y = d (the beginning of Region 2). l_a , Δy , Y^* , l_d and L denote the adsorption length, width of the bulk solution concentration

gradient, width of the surface concentration gradient, width of the optically extinct area and width of the LC film, respectively. (c) Variation of surface concentration of SDS and aqueous-LC interfacial velocity as a function of distance across Region 2 as predicted by the physical model for a LC film exposed experimental conditions described in Fig. 2e. Measured values of the surface velocity at various locations of the interface in Region 2 are plotted alongside the model surface velocities. Error bar for measure v_s : S.D. with n=3. (d) Influence of $\Delta \pi_{eq}$ on the optical response of LC between crossed polars. (e) A plot of interfacial velocities (model and measured) versus $\Delta \pi_{eq}$. Error bar: S.D. with n=3.

Region 2: In Region 2, the interface of the LC is exposed to a concentration of SDS in bulk solution that decreases with increase in y. As discussed above, we propose that a gradient in interfacial SDS concentration is generated in Region 2 and that this leads to a Marangoni flow away from Region 1. To determine the relative importance of surface advection and surface diffusion in Region 2, we calculated a surface Peclet number, Pes, defined as the ratio of surface diffusion time to surface advection time. We define the y-axis in Region 2 as Y = (y-d) as shown in Fig. 5b. The surface diffusion time is expressed as Y*2/Ds, where Y* is the width of the surface concentration gradient (which is bounded in magnitude by the width of the bulk solution concentration gradient ($\Delta y \sim 40 \mu m$) and the width of the Region 2 (~ ((285-40) μ m/2)+40 μ m = 163 μ m, assuming the external gradient in SDS concentration is located at the middle of the square LC film) and Ds $\sim 10^{-10}$ m²/s is the surface diffusion coefficient of SDS⁷⁴. The surface advection time is expressed as Y*/vs, where $v_s = 30 \mu m/s$ is a characteristic interfacial velocity (see SI). We calculated the Pes to vary between 12 and 49, indicating that surface transport of surfactant is dominated by advection (over diffusion). We use this result below to develop a simple model that describes the interfacial surfactant concentration profile across Region 2 of LC interface.

To describe the evolution of the SDS concentration gradient across Region 2, and the associated interfacial velocity that results from the Marangoni stress, we determined the characteristic time for desorption of SDS in the presence of 300 mM NaCl. By using the pendant drop method, we determined it to be 50 s (details in SI). Because the characteristic times for surface advection (Y*/v_s ~ 163 $\mu m/(30~\mu m/s) \sim 5.5$ s, see above) and desorption of SDS (~50 s) are comparable, we conclude that the surfactant coverage across the LC interface in our experiments will be

dominated by these two processes. Accordingly, we describe the evolution of the interfacial surfactant concentration in Region 2 of the aqueous-LC interface as ¹

$$\nabla_{s.}(v_{s}\Gamma) = -k_{d}(\Gamma - \Gamma_{eq\,2}) \tag{1}$$

where V_s is the surface (Y-direction) gradient and Γ_{eq2} is the surface concentration of SDS in equilibrium with the bulk SDS solution on the low concentration side of the aqueous-LC interface (Fig. 5b). Due to slow desorption of SDS from the interface (see above), the surface concentration of SDS in Region 2 will be higher than the local equilibrium surface concentration, Γ_{eq2} . At steady-state, the Marangoni stress at the aqueous-LC interface will be balanced by the viscous stress due to shearing of the LC film, which we write as

$$\frac{d\gamma}{dY} = \eta \frac{dv}{dz} \tag{2}$$

where γ is the interfacial tension of 5CB with the aqueous SDS solution, η is the average viscosity of 5CB (approximated as an isotropic phase with a viscosity of 30 mPa·s⁷⁵) and v is the velocity of 5CB, and z is the direction across the thickness of the LC film (see Fig. 5a).

To express γ (in Equation 2) in terms of Γ , we measured γ of the aqueous-5CB interface at different bulk concentrations of SDS in aqueous solution (in presence of 300 mM NaCl) and used the Gibbs adsorption isotherm to estimate Γ (e.g., for a bulk SDS concentration of 0.5 mM in 300 mM NaCl, we measured γ to be 4.30 ± 0.02 mN/m and estimated Γ to be 4.43×10^{-6} mol/m²; see SI for detail). We found γ to vary linearly with Γ over the experimental conditions relevant to our experiments. To simplify the model, we assume a linear velocity profile of 5CB across the film thickness 26 with a no-slip boundary condition at the solid boundary (z = 0) and v = v_s at the aqueous interface (z = t_Lc, the thickness of the film of 5CB). The above simplifications allow us to rewrite Equation 2 as

$$\frac{d\Gamma}{dY} = -\frac{\eta v_s}{a t_{LC}} \tag{3}$$

where a = 2845 N/mol is the slope of the plot of γ vs Γ (see SI).

As discussed above, the leading end of Region 1 (Y = 0; see Fig. 5b for the definition of y = 0) remains in equilibrium with the bulk solution of high SDS concentration, which can be written as

$$\Gamma = \Gamma_{eq\ 2} \ at \ Y = 0 \tag{4}$$

Moreover, the presence of the grid wall at Y = L requires that

$$\frac{d\Gamma}{dY} = 0 \text{ at } Y = L \tag{5}$$

Fig. 5c shows the solution to Equations 1 and 3 (see SI for details) using the boundary conditions shown in Equations 4 and 5. Inspection of Fig. 5c reveals a quadratic decay of Γ as a function of Y in Region 2. Fig. 5c also reveals that the difference in Γ between the two ends of Region 2 at steady state, $\Delta\Gamma_{ss}$ (= Γ_{eq1} - Γ_{L-d} ~ $2.73~\times~10^{-9}~mol/m^2\text{,}~\Gamma_{L\text{-}d}~being~the~surface$ concentration of SDS at Y = (L-d) at steady state) is much smaller than the difference in surface concentration of SDS at equilibrium with aqueous solutions of high and low concentrations of SDS used in the experiment, $\Delta\Gamma_{eq}$ (= Γ_{eq1} - Γ_{eq2} \sim 2.01 \times 10^{-6} mol/m²). Moreover, the interfacial concentration gradient persists over a lateral distance (L-d), a distance that is much larger than the width of the bulk solution concentration gradient, Δy (see Fig. 5b). This prediction is qualitatively consistent with our experimental observation that the optical response of the LC extends over a spatial distance that is much larger than the imposed bulk solution gradient in concentration (see Fig. 2e,f). The model also predicts a continuous decrease in surface velocity across the LC interface in Region 2 (Figure 5c). Although the model prediction (almost linear change in velocity) differs from the experimental observation (parabolic change in velocity), given the simplifying assumptions underlying the model, the general agreement between the model and experiment is viewed as satisfactory. In addition, we found that our simple model provided an account of the variation of surface velocity with the magnitude of external gradient in SDS concentration that we observed in our experiments (Fig. 5d; see Fig. S7 for the corresponding optical images of LC). Overall, these results indicate that the interfacial surfactant coverage and surface velocity of the LC in Region 2 are largely governed by an interplay between surface advection and surfactant desorption kinetics.

As noted above, past studies have established that a change in surface concentration of a surfactant can change the orientation of a LC at the aqueous interface 69 . It is possible, therefore, that the spatial variation of Γ , as predicted by the above model, could also induce a variation in the orientation of the LC. However, our analysis leads us to conclude that this effect is small in our experiments. Specifically, at equilibrium, we estimated the maximum surface concentration of SDS that can sustain a tilt of LC away from the surface normal (causing a non-zero optical retardance of 5CB) to be $1.09\times 10^{-6}~\text{mol/m}^2$ (this corresponds to a SDS concentration of 0.016 mM in 300 mM NaCl in the bulk aqueous solution), which is much lower than the above-described estimated

values of $\Gamma_{L\text{-}d}$ (as well as the measured value of Γ_{eq2}). In addition, as discussed in SI, the impact of the variation in SDS surface concentration on the surface anchoring energy of the LC is very small under the experimental conditions reported in this paper.

We conclude this section by noting that the surface flow in Region 2 drives a circulatory flow within the LC film, including in Region 1. The presence of the circulatory flow in Region 1 leads to a tilting of the LC away from the surface normal, and thus the optical retardance evident in Figures 2f and 3a.

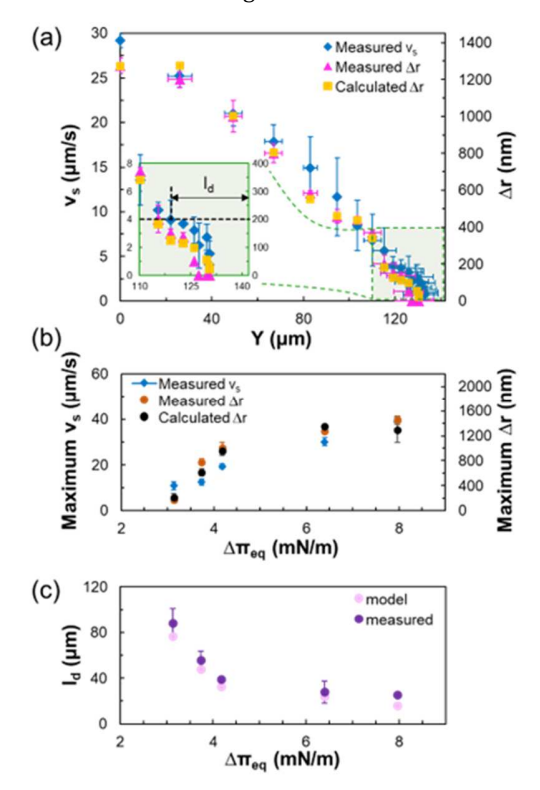


Fig. 6. (a) A plot of measured surface velocity and measured and calculated optical retardance of LC films exposed experimental concentration described in Fig. 2e. Inset (green box in the bottom left corner) shows a magnified plot at high y (near the solid wall). Error bar: S.D. with n = 3. (b) Variation of maximum surface velocity and maximum optical retardance (measured and calculated) of the LC films with $\Delta\pi_{eq}$. Error bar: S.D. with n = 3. (c) A plot of the width of the optically dark region (model and measured) near the confining walls of the LC films towards the low concentration side (y = L) versus $\Delta\pi_{eq}$. Error bar: S.D. with n = 3.

3.5 LC optical response to interfacial flows

To describe the optical response of the LC to the SDS gradients observed in our experiments, we equated torques arising from the elastic strain of the LC film

and the anisotropic viscosities of the sheared LC, ^{26,27} namely

$$K_{LC}\left(\frac{d^2\theta}{dz^2}\right) = \left(\frac{dv_s}{dz}\right)(\alpha_2 cos^2\theta - \alpha_3 sin^2\theta) \tag{6}$$

where, $K_{LC} \sim \! 10^{\text{-}11}$ N is the average elastic constant of the LC (using one parameter approximation), $\alpha_2 \sim -83$ \times 10⁻³ kg/ms and $\alpha_3 \sim$ - 2 \times 10⁻³ kg/ms are the Leslie viscosity coefficients of 5CB²⁶, v_s is the aqueous-LC interfacial velocity (along y), and θ is the angle of tilt of LC from the surface normal. For the tilt angle profiles calculated using Equation 6, we calculated the corresponding values of the optical retardance of the LC films (see SI for details). Specifically, by using the interfacial velocities predicted by the above-described model between y = 0 and y = (L-d) (see Fig. 5c), we calculated Δr of the LC film, and compared it to experimental measurements (Fig. 6a). The general agreement between the experiment and model shown in Fig. 6a provides additional support for our conclusion that the optical response of the LC is dominated by a shear-induced reorganization. Additionally, Fig. 6a shows that the LC optical retardance correlates very closely with the surface velocity along the LC interface hinting at the potential use of the LC optical response as a convenient way to map surface flows. We also found good agreement between experiment and model when the magnitude of the SDS gradient was varied (Fig. 6b).

Fig. 3 reveals that the LC films exposed to SDS gradients exhibit a dark optical appearance near the grid wall in Region 2 (corresponding to an optical retardance of less than 200 nm). Inspection of Fig. 6a reveals that the surface velocity in the abovementioned region of the interface is less than or equal to 4 μ m/s. At or below this minimum v_s , the interfacial flow-induced shear is insufficient to cause a measurable tilting of LC away from the surface normal (i.e., $\Delta r < 200$ nm for optically dark appearance, see SI for details). We calculated the distance from the grid wall (ld, see Fig. 5d for the definition) at which the LC surface velocity decreased to 4 µm/s as a function of the magnitude of the SDS gradients. A plot of l_{d} as a function of $\Delta \pi_{eq}$ (Fig. 6c) reveals good agreement between experiment and the model prediction.

3.6 The effects of confinement on the LC optical response to surfactant concentration gradients

As described above, the presence of the grid wall at Y = (L-d) confines the interfacial flow and thus plays an important role in the establishment of the flow by imposing a no-slip boundary condition. This brings us

to the prediction that an increase in the size of LC films in the direction of the interfacial flows (L) will cause an increase in $\Delta\Gamma_{ss}$ and v_s which will generate a higher deviation of LC from the surface normal (Equation 6) causing an increase in Δr . Therefore, key prediction that emerges from the model described above is that an amplified and stronger (higher optical retardance) LC response will be observed with an increase in the LC domain size. Here we explore that prediction. As shown in Fig. 7, we performed experiments with five TEM grids with lateral slot lengths of 58 μm , 205 μm , 285 μm , 420 μm , and 1 mm, and exposed them to the same SDS concentration gradient (see caption of Fig. 7 for details).

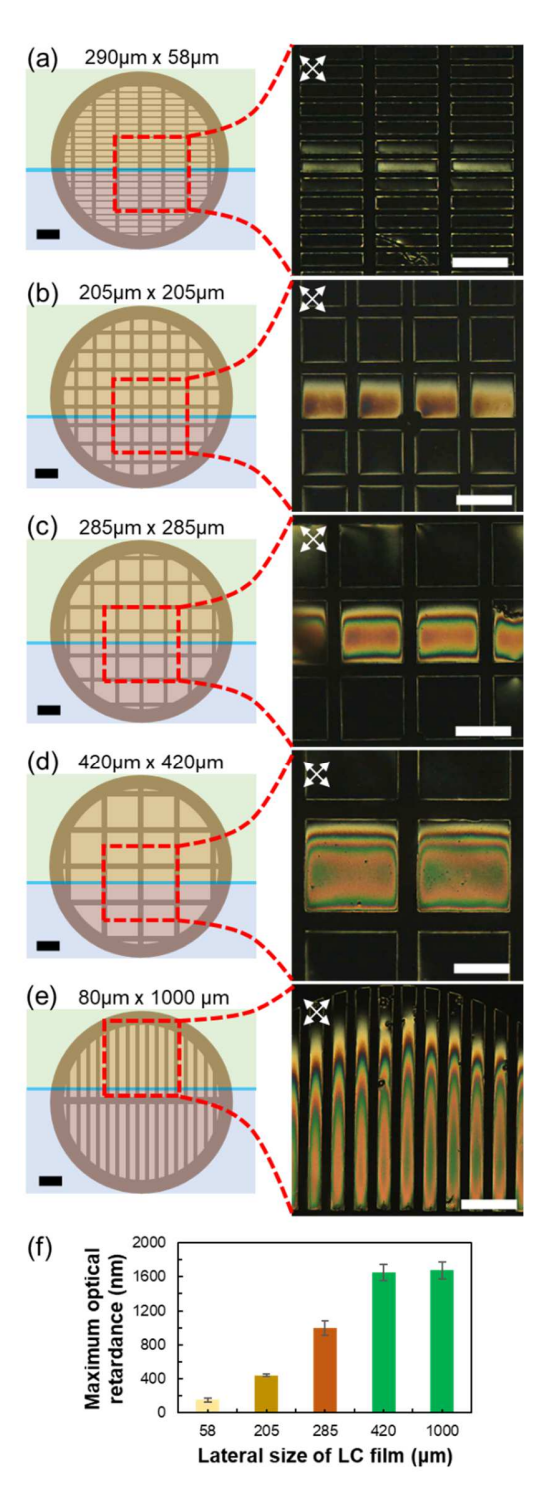


Fig. 7. Amplification of the spatial response of LC: LC films of different lateral sizes are placed under the same gradient conditions (containing 0.5 mM and 0.25 mM SDS solutions (color-coded blue and green, respectively) pumped at a flow rate of 2 mL/min each) and the optical responses of the LC films in the square areas enclosed by red dotted outlines are observed between crossed polars.

Planar dimensions of the LC grids are (a) 290 μm x 58 μm ; (b) 205 μm x 205 μm ; (c) 285 μm x 285 μm ; (d) 420 μm x 420 μm ; (e) 80 μm x 1 mm. Scale bars are 250 μm . (f) A plot of maximum optical retardance observed near the middle of the bright LC responses with the lateral size of the LC films. Error bar: S.D. with n = 3.

Inspection of Fig. 7 reveals a systematic increase in optical retardance (maximum optical retardance near the middle of the bright LC responses) with the increase in the size of the LC domain. The increase in the optical retardance (from ~ 450 nm to 1500 nm; Fig. 7f) reflects an increase in the aqueous-LC interfacial velocity with LC domain size (from 16 $\mu m/s$ to 40 $\mu m/s$). This provides support for our conclusion that the difference in $\boldsymbol{\Gamma}$ between the two ends of Region 2, $\Delta\Gamma_{ss}$ increases with the size of Region 2, which causes an increased surface velocity and thus a higher LC optical retardance. Overall, these results demonstrate LC amplification of the spatial extent of surfactant concentration gradients by as much as 25X. This hints at the potential use of LCs to magnify microscale gradients into macro-scale optical responses for easy characterization.

3.7 Transport and localization of microparticles at aqueous-LC interfaces driven by surfactant concentration gradients

As described above, to characterize the LC velocity in the presence of surfactant concentration gradients, we dispersed silica microparticles (diameter 3 µm) in the LC films and tracked their displacement. In the course of these measurements, in addition to observing the presence of isolated microparticles that exhibit a circulatory motion, we made the unanticipated observation of the formation of near-stationary interfacially-trapped assemblies of particles (Fig. 8c,d). Specifically, the microparticles, initially present in the bulk of the LC film (Fig. 8a) at a concentration of 1% wt/vol, when exposed to a gradient in SDS concentration (consisting of 0.5 mM and 0.25 mM SDS solutions in 300 mM NaCl and pumped at an overall flow rate of 1 mL/min), were transported to the interface as singly dispersed particles by the circulatory motion of the LC. Upon reaching the aqueous-LC interface, the microparticles interacted with each other to form chains (Fig. 8b) with most of the chaining events occurring in the direction of the interfacial flow (Fig. 8c). Subsequently, the chains rotated by an angle of $\sim 30^{\circ}$ away from the direction of the interfacial flow (Fig. 8d; see inset for details) and localized near the middle of the interface (the region of the interface with the highest optical retardance). The above-described process was observed to occur within

the first few minutes (typically, 2 minutes) of the establishment of a steady state flow field inside the LC domain. Additionally, the linear chains of microparticles were observed to interact with each other forming 2D interfacially-trapped assemblies of microparticles (Fig. S12).

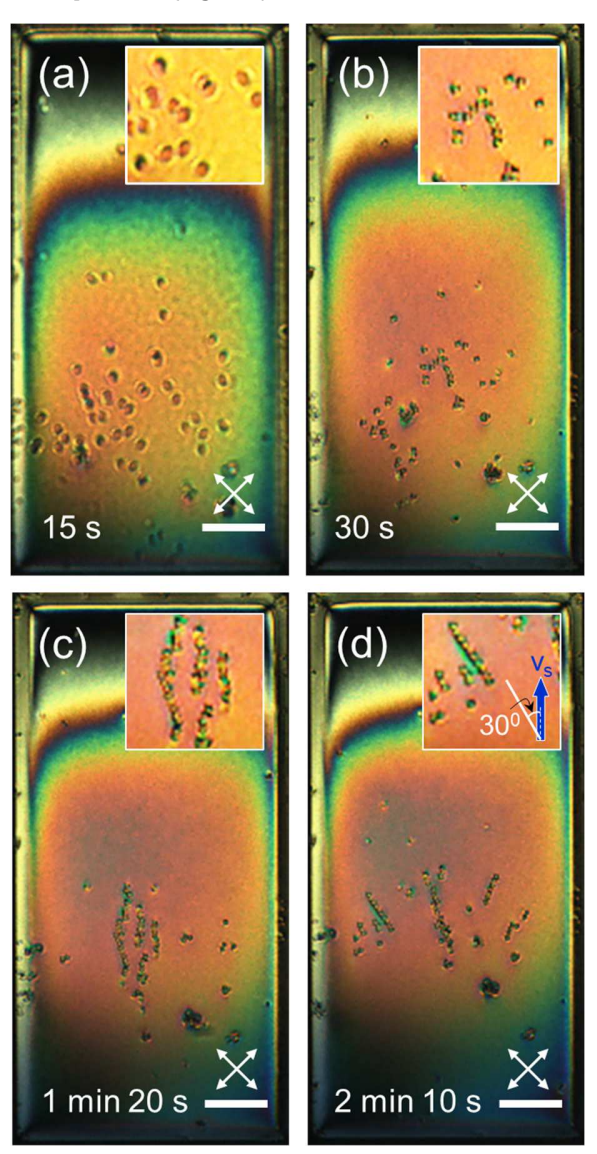


Fig. 8. (a-d) Time-series images of the formation and localization of assemblies of silica microparticles at aqueous-LC interface. A film of 5CB with dispersed silica particles of diameter 3 μm is placed inside a milli-fluidic channel containing a gradient in SDS concentration generated by pumping solutions of 0.5 mM and 0.25 mM SDS in 300 mM NaCl at an overall flow rate of 1 mL/min. Insets show magnified views of the organizations of particles in the corresponding images. Scale bars are 50 μm .

We propose that the above-described localization of the microparticles at the LC interface reflects a coupling between the flow-induced strain of the LC (tilting away from surface normal) and the strain of the LC around the microparticles. Specifically, silica microparticles induce a tangential anchoring of 5CB (Fig. S9) leading to the presence of two surface boojum defects and elastic quadrupolar interactions⁷⁶ between the interfacially-trapped microparticles. We propose that the maximum in LC interfacial velocity coincides with the highest elastic free energy density in the LC film which drives the interfacial chains of microparticles to preferentially localize in these regions. Support for this proposition comes from experiments performed with isotropic oils, which did not lead to localization of the microparticles (see SI). Although additional studies are needed to fully understand this phenomenon, this initial set of observations hints that Marangoni flow-driven nonequilibrium states of organization of LCs can cause microparticles into localize on interfaces in ways that are not observed with isotropic liquids.

4. Conclusions

This paper reports on the non-equilibrium ordering of LC films in response to external gradients in surfactant concentration. We generate gradients in surfactant concentration by introducing two streams containing different concentrations of surfactant into a milli-fluidic channel containing a LC film. By examining the optical response of the LC film, we show how this experimental set-up permits manipulation of the surface gradients in surfactant concentration. We find that the optical retardance of the LC film correlates closely with the magnitude of the surfactant concentration gradient generated using the millifluidic channel. In contrast to particle trackingmethods, a single image of the LC can be used to determine the interfacial flow field generated by the surfactant concentration gradients. This allows facile identification of regions of the LC interface where the surface gradients are located, and phenomena such as immobilization of the interface by high surfactant concentrations (down-stream region of the interface). By varying the size of the LC domain and mapping the interfacial velocity using the LC, we show that the width of the surface concentration of the surfactants **References:**

can exceed the spatial extent of the bulk concentration gradient by a factor of 25, thus revealing that LC optical responses that provide a means to magnify microscopic gradients into large-scale optical responses that are readily characterized. Overall, we conclude that LCs provide a convenient and simple method for characterizing microscopic gradients in surfactant concentration and mapping interfacial velocities.

The results discussed in this paper generate a number of questions that deserve future investigation. First, although we explore the effect of the size of the rectangular LC domain on the LC optical response, we do not yet understand how non-rectangular domains with converging and diverging surface areas in the direction parallel to the surfactant concentration gradient impact the magnitudes of the surface concentration gradients and optical response. Second, our interpretation of the optical response of the LC assumes a linear velocity profile across the thickness of the LC film. However, the behavior of microparticles in our experiments reveal that the LC undergoes a circulatory flow. Additional modeling of the fluid mechanics is needed to more fully account for the influence of this circulation on the optical response of the LC. Third, we observed solid microparticles to form organized assemblies at the interface of the LC films in the presence of the surfactant concentration gradients. Our preliminary experiments hint that these assemblies reflect the interaction of the LC strain fields around the microparticles and regions of the LC film strained by the interfacial flows. Additional experiments are needed to fully understand the nonequilibrium forces that generate these microparticle assemblies.

Acknowledgements

We acknowledge support from the National Science Foundation (CBET-1803409 and EFMA1935252) and the Army Research Office through W911NF-15-1-0568 and W911NF-17-1-0575. This work was performed in part at the Cornell NanoScale Facility, a member of the National Nanotechnology Coordinated Infrastructure (NNCI), which is supported by the National Science Foundation (Grant NNCI-2025233). We thank Alyssa B. Apsel and Hadas Kress-Gazit for insightful comments and discussions.

(1) Manikantan, H.; Squires, T. M. Surfactant Dynamics: Hidden Variables Controlling Fluid Flows. *J Fluid Mech* **2020**, *892*, 1–115. https://doi.org/10.1017/jfm.2020.170.

- (2) Stebe, K. J.; Maldarelli, C. Remobilizing Surfactant Retarded Fluid Particle Interfaces. II. Controlling the Surface Mobility at Interfaces of Solutions Containing Surface Active Components. *Journal of Colloid And Interface Science*. 1994, pp 177–189. https://doi.org/10.1006/jcis.1994.1094.
- (3) Chen, J.; Stebe, K. J. Marangoni Retardation of the Terminal Velocity of a Settling Droplet: The Role of Surfactant Physico-Chemistry. *J Colloid Interface Sci* **1996**, *178* (1), 144–155. https://doi.org/10.1006/jcis.1996.0102.
- (4) Chen, C. V. H. H.; Liu, Y.; Stone, H. A.; Prud'Homme, R. K. Visualization of Surfactant Dynamics to and along Oil-Water Interfaces Using Solvatochromic Fluorescent Surfactants. *Langmuir* **2018**, *34* (36), 10512–10522. https://doi.org/10.1021/acs.langmuir.8b01740.
- (5) Eggleton, C. D.; Tsai, T. M.; Stebe, K. J. Tip Streaming from a Drop in the Presence of Surfactants. *Phys Rev Lett* **2001**, *87* (4), 48302-148302-48304. https://doi.org/10.1103/PhysRevLett.87.048302.
- (6) Sinz, D. K. N.; Darhuber, A. A. Self-Propelling Surfactant Droplets in Chemically-Confined Microfluidics -Cargo Transport, Drop-Splitting and Trajectory Control. *Lab Chip* 2012, 12 (4), 705–707. https://doi.org/10.1039/c2lc21082g.
- (7) Jin, C.; Kru-ger, C.; Maass, C. C. Chemotaxis and Autochemotaxis of Self-Propelling Droplet Swimmers. *Proc Natl Acad Sci U S A* **2017**, *114* (20), 5089–5094. https://doi.org/10.1073/pnas.1619783114.
- (8) Daniel, S.; Chaudhury, M. K.; Chen, J. C. Fast Drop Movements Resulting from the Phase Change on a Gradient Surface. *Science* (1979) **2001**, 291 (5504), 633–636. https://doi.org/10.1126/science.291.5504.633.
- (9) dos Santos, F. D.; Ondarçuhu, T. Free-Running Droplets. *Phys Rev Lett* **1995**, *75* (16), 2972. https://doi.org/10.1103/PhysRevLett.75.2972.
- (10) Hamraoui, A.; Cachile, M.; Poulard, C.; Cazabat, A. M. Fingering Phenomena during Spreading of Surfactant Solutions. *Colloids Surf A Physicochem Eng Asp* **2004**, *250* (1-3 SPEC. ISS.), 215–221. https://doi.org/10.1016/j.colsurfa.2003.12.035.
- (11) Warner, M. R. E.; Craster, R. V.; Matar, O. K. Fingering Phenomena Associated with Insoluble Surfactant Spreading on Thin Liquid Films. *J Fluid Mech* **2004**, *510* (510), 169–200. https://doi.org/10.1017/S0022112004009437.
- (12) Edmonstone, B. D.; Craster, R. V.; Matar, O. K. Surfactant-Induced Fingering Phenomena beyond the Critical Micelle Concentration; 2006; Vol. 564. https://doi.org/10.1017/S0022112006001352.
- (13) Matar, O. K.; Troian, S. M. The Development of Transient Fingering Patterns during the Spreading of Surfactant Coated Films. *Physics of Fluids* **1999**, *11* (11), 3232–3246. https://doi.org/10.1063/1.870185.
- (14) Matar, O. K.; Craster, R. V. Dynamics of Surfactant-Assisted Spreading. **2009**, 3801–3809. https://doi.org/10.1039/b908719m.
- (15) Troian, S. M.; Wu, X. L.; Safran, S. A. Fingering Instability in Thin Wetting Films. *Phys Rev Lett* **1989**, *62* (13), 1496. https://doi.org/10.1103/PhysRevLett.62.1496.
- (16) Troian, S. M.; Herbolzheimer, E.; Safran, S. A. Model for the Fingering Instability of Spreading Surfactant Drops. *Phys Rev Lett* **1990**, *65* (3), 333. https://doi.org/10.1103/PhysRevLett.65.333.
- (17) Zarzar, L. D.; Sresht, V.; Sletten, E. M.; Kalow, J. A.; Blankschtein, D.; Swager, T. M. Dynamically Reconfigurable Complex Emulsions via Tunable Interfacial Tensions. *Nature* **2015**, *518* (7540), 520–524. https://doi.org/10.1038/nature14168.
- (18) Karapetsas, G.; Sahu, K. C.; Matar, O. K. Evaporation of Sessile Droplets Laden with Particles and Insoluble Surfactants. *Langmuir* **2016**, *32* (27), 6871–6881. https://doi.org/10.1021/acs.langmuir.6b01042.

- (19) Mampallil, D.; Eral, H. B. A Review on Suppression and Utilization of the Coffee-Ring Effect. *Adv Colloid Interface Sci* **2018**, *252*, 38–54. https://doi.org/10.1016/j.cis.2017.12.008.
- (20) Starov, V. M.; De Ryck, A.; Velarde, M. G. On the Spreading of an Insoluble Surfactant over a Thin Viscous Liquid Layer. *J Colloid Interface Sci* **1997**, *190* (1), 104–113. https://doi.org/10.1006/jcis.1997.4863.
- (21) Bull, J. L.; Grotberg, J. B. Surfactant Spreading on Thin Viscous Films: Film Thickness Evolution and Periodic Wall Stretch. *Exp Fluids* **2003**, *34* (1), 1–15. https://doi.org/10.1007/s00348-002-0447-2.
- (22) Fallest, D. W.; Lichtenberger, A. M.; Fox, C. J.; Daniels, K. E. Fluorescent Visualization of a Spreading Surfactant. *New J Phys* **2010**, *12*. https://doi.org/10.1088/1367-2630/12/7/073029.
- (23) Song, Q.; Yuan, M. Visualization of an Adsorption Model for Surfactant Transport from Micelle Solutions to a Clean Air/Water Interface Using Fluorescence Microscopy. *J Colloid Interface Sci* **2011**, *357* (1), 179–188. https://doi.org/10.1016/j.jcis.2011.01.096.
- (24) Hosokawa, S.; Masukura, Y.; Hayashi, K.; Tomiyama, A. Experimental Evaluation of Marangoni Stress and Surfactant Concentration at Interface of Contaminated Single Spherical Drop Using Spatiotemporal Filter Velocimetry. *International Journal of Multiphase Flow* **2017**, *97*, 157–167. https://doi.org/10.1016/j.ijmultiphaseflow.2017.08.007.
- (25) Eftekhari, M.; Schwarzenberger, K.; Heitkam, S.; Eckert, K. Interfacial Flow of a Surfactant-Laden Interface under Asymmetric Shear Flow. *J Colloid Interface Sci* **2021**, *599*, 837–848. https://doi.org/10.1016/j.jcis.2021.04.126.
- (26) Tsuei, M.; Shivrayan, M.; Kim, Y. K.; Thayumanavan, S.; Abbott, N. L. Optical "Blinking" Triggered by Collisions of Single Supramolecular Assemblies of Amphiphilic Molecules with Interfaces of Liquid Crystals. *J Am Chem Soc* **2020**, *142* (13), 6139–6148. https://doi.org/10.1021/jacs.9b13360.
- (27) Roh, S.; Tsuei, M.; Abbott, N. L. Using Liquid Crystals for in Situ Optical Mapping of Interfacial Mobility and Surfactant Concentrations at Flowing Aqueous-Oil Interfaces. *Langmuir* **2021**, *37* (19), 5810–5822. https://doi.org/10.1021/acs.langmuir.1c00133.
- (28) Kim, Y. K.; Wang, X.; Mondkar, P.; Bukusoglu, E.; Abbott, N. L. Self-Reporting and Self-Regulating Liquid Crystals. *Nature 2018 557:7706* **2018**, *557* (7706), 539–544. https://doi.org/10.1038/s41586-018-0098-y.
- (29) Kim, Y. K.; Huang, Y.; Tsuei, M.; Wang, X.; Gianneschi, N. C.; Abbott, N. L. Multi-Scale Responses of Liquid Crystals Triggered by Interfacial Assemblies of Cleavable Homopolymers. *ChemPhysChem* **2018**, *19* (16), 2037–2045. https://doi.org/10.1002/cphc.201800106.
- (30) Carlton, R. J.; Ma, C. D.; Gupta, J. K.; Abbott, N. L. Influence of Specific Anions on the Orientational Ordering of Thermotropic Liquid Crystals at Aqueous Interfaces. *Langmuir* **2012**, *28* (35), 12796–12805. https://doi.org/10.1021/la3024293.
- (31) Wang, X.; Yang, P.; Mondiot, F.; Li, Y.; Miller, D. S.; Chen, Z.; Abbott, N. L. Interfacial Ordering of Thermotropic Liquid Crystals Triggered by the Secondary Structures of Oligopeptides. *Chemical Communications* **2015**, *51* (94), 16844–16847. https://doi.org/10.1039/c5cc06996c.
- (32) Zhou, J.; Dong, Y.; Zhang, Y.; Liu, D.; Yang, Z. The Assembly of DNA Amphiphiles at Liquid Crystal-Aqueous Interface. *Nanomaterials* **2016**, *6* (12). https://doi.org/10.3390/nano6120229.
- (33) Popov, P.; Mann, E. K.; Jákli, A. Thermotropic Liquid Crystal Films for Biosensors and Beyond. *J Mater Chem B* **2017**, *5* (26), 5061–5078. https://doi.org/10.1039/c7tb00809k.
- (34) Carlton, R. J.; Hunter, J. T.; Miller, D. S.; Abbasi, R.; Mushenheim, P. C.; Tan, L. N.; Abbott, N. L. Chemical and Biological Sensing Using Liquid Crystals. *Liq Cryst Rev* **2013**, *1* (1), 29–51. https://doi.org/10.1080/21680396.2013.769310.

- (35) Daschner De Tercero, M.; Abbott, N. L. Ordering Transitions in Liquid Crystals Permit Imaging of Spatial and Temporal Patterns Formed by Proteins Penetrating into Lipid-Laden Interfaces. *Chem Eng Commun* **2009**, 196 (1–2), 234–251. https://doi.org/10.1080/00986440802290060.
- (36) Brake, J. M.; Abbott, N. L. An Experimental System for Imaging the Reversible Adsorption of Amphiphiles at Aqueous-Liquid Crystal Interfaces. *Langmuir* **2002**, *18* (16), 6101–6109. https://doi.org/10.1021/la011746t.
- (37) Brake, J. M.; Mezera, A. D.; Abbott, N. L. Effect of Surfactant Structure on the Orientation of Liquid Crystals at Aqueous-Liquid Crystal Interfaces. *Langmuir* **2003**, *19* (16), 6436–6442. https://doi.org/10.1021/la034132s.
- (38) Tian, T.; Kang, Q.; Wang, T.; Xiao, J.; Yu, L. Alignment of Nematic Liquid Crystals Decorated with Gemini Surfactants and Interaction of Proteins with Gemini Surfactants at Fluid Interfaces. *J Colloid Interface Sci* **2018**, *518*, 111–121. https://doi.org/10.1016/j.jcis.2018.02.027.
- (39) Adamiak, L.; Pendery, J.; Sun, J.; Iwabata, K.; Gianneschi, N. C.; Abbott, N. L. Design Principles for Triggerable Polymeric Amphiphiles with Mesogenic Side Chains for Multiscale Responses with Liquid Crystals. *Macromolecules* **2018**, *51* (5), 1978–1985. https://doi.org/10.1021/acs.macromol.7b02140.
- (40) Brake, J. M.; Daschner, M. K.; Abbott, N. L. Formation and Characterization of Phospholipid Monolayers Spontaneously Assembled at Interfaces between Aqueous Phases and Thermotropic Liquid Crystals. *Langmuir* **2005**, *21* (6), 2218–2228. https://doi.org/10.1021/la0482397.
- (41) Bukusoglu, E.; Pantoja, M. B.; Mushenheim, P. C.; Wang, X.; Abbott, N. L. Design of Responsive and Active (Soft) Materials Using Liquid Crystals. *Annu Rev Chem Biomol Eng* **2016**, *7*, 163–196. https://doi.org/10.1146/annurev-chembioeng-061114-123323.
- (42) Tsang, N.; Macnab, R.; Koshland, D. E. Common Mechanism for Repellents and Attractants in Bacterial Chemotaxis. *Science* (1979) **1973**, 181 (4094), 60–61. https://doi.org/10.1126/science.181.4094.60.
- (43) Schneider, I. C.; Haugh, J. M. Mechanisms of Gradient Sensing and Chemotaxis: Conserved Pathways, Diverse Regulation. *Cell Cycle* **2006**, *5* (11), 1130–1134. https://doi.org/10.4161/cc.5.11.2770.
- (44) Hu, B.; Chen, W.; Rappel, W. J.; Levine, H. Physical Limits on Cellular Sensing of Spatial Gradients. *Phys Rev Lett* **2010**, *105* (4), 1–4. https://doi.org/10.1103/PhysRevLett.105.048104.
- (45) Macnab, R. M.; Koshland, D. E. The Gradient-Sensing Mechanism in Bacterial Chemotaxis. *Proc Natl Acad Sci U S A* **1972**, *69* (9), 2509–2512. https://doi.org/10.1073/pnas.69.9.2509.
- (46) Endres, R. G.; Wingreen, N. S. Accuracy of Direct Gradient Sensing by Cell-Surface Receptors. *Prog Biophys Mol Biol* **2009**, *100* (1–3), 33–39. https://doi.org/10.1016/j.pbiomolbio.2009.06.002.
- (47) Ma, L. Y.; Wang, H. Y.; Xie, H.; Xu, L. X. A Long Lifetime Chemical Sensor: Study on Fluorescence Property of Fluorescein Isothiocyanate and Preparation of PH Chemical Sensor. *Spectrochim Acta A Mol Biomol Spectrosc* **2004**, *60* (8–9), 1865–1872. https://doi.org/10.1016/j.saa.2003.10.004.
- (48) Li, P.; Martin, C. M.; Yeung, K. K.; Xue, W. Dielectrophoresis Aligned Single-Walled Carbon Nanotubes as Ph Ensors. *Biosensors (Basel)* **2011**, *1* (1), 23–35. https://doi.org/10.3390/bios1010023.
- (49) Gou, P.; Kraut, N. D.; Feigel, I. M.; Bai, H.; Morgan, G. J.; Chen, Y.; Tang, Y.; Bocan, K.; Stachel, J.; Berger, L.; Mickle, M.; SejdiĆ, E.; Star, A. Carbon Nanotube Chemiresistor for Wireless PH Sensing. *Sci Rep* **2014**, *4*, 1–6. https://doi.org/10.1038/srep04468.
- (50) Takeda, S.; Nakamura, M.; Ishii, A.; Subagyo, A.; Hosoi, H.; Sueoka, K.; Mukasa, K. A PH Sensor Based on Electric Properties of Nanotubes on a Glass Substrate. *Nanoscale Res Lett* **2007**, *2* (4), 207–212. https://doi.org/10.1007/s11671-007-9053-9.

- (51) Falciai, R.; Mignani, A. G.; Vannini, A. Long Period Gratings as Solution Concentration Sensors. *Sens Actuators B Chem* **2001**, *74* (1–3), 74–77. https://doi.org/10.1016/S0925-4005(00)00714-0.
- (52) Bhatia, R.; Dilleen, J. W.; Atkinson, A. L.; Rawson, D. M. Combined Physico-Chemical and Biological Sensing in Environmental Monitoring. *Biosens Bioelectron* **2003**, *18* (5–6), 667–674. https://doi.org/10.1016/S0956-5663(03)00012-5.
- (53) Su, H.; Huang, X. G. Fresnel-Reflection-Based Fiber Sensor for on-Line Measurement of Solute Concentration in Solutions. *Sens Actuators B Chem* **2007**, *126* (2), 579–582. https://doi.org/10.1016/j.snb.2007.04.008.
- (54) Islama, M. R.; Serpe, M. J. Polyelectrolyte Mediated Intra and Intermolecular Crosslinking in Microgel-Based Etalons for Sensing Protein Concentration in Solution. *Chemical Communications* **2013**, 49 (26), 2646–2648. https://doi.org/10.1039/c3cc00211j.
- (55) Yang, M. H.; Lohani, C. R.; Cho, H.; Lee, K. H. A Methionine-Based Turn-on Chemical Sensor for Selectively Monitoring Hg2+ Ions in 100% Aqueous Solution. *Org Biomol Chem* **2011**, *9* (7), 2350–2356. https://doi.org/10.1039/c0ob00780c.
- (56) Wiskur, S. L.; Floriano, P. N.; Anslyn, E. V.; McDevitt, J. T. A Multicomponent Sensing Ensemble in Solution: Differentiation between Structurally Similar Analytes. *Angewandte Chemie International Edition* **2003**, *42* (18), 2070–2072. https://doi.org/10.1002/anie.200351058.
- (57) Mandelis, A.; Dignam, M. J.; Pawliszyn, J.; Weber, M. F.; Park, S. M.; Venter, R. D. Observation of Concentration Gradients by the Laser Beam Deflection Sensor. *Anal Chem* **1986**, *58* (1), 236–239. https://doi.org/10.1021/ac00292a058.
- (58) Mandelis, A.; Dignam, M. J.; Pawliszyn, J.; Weber, M. F.; Park, S. M.; Venter, R. D. Selective Observation of Concentration Gradients by the Laser Beam Deflection Sensor Applied to in Situ Electrochemical Studies. A Novel Approach. *Anal Chem* **1986**, *58* (1), 239–242. https://doi.org/10.1021/ac00292a059.
- (59) Pawliszyn, J. Properties and Applications of the Concentration Gradient Sensor to Detection of Flowing Samples. *Anal Chem* **1986**, *58* (14), 3207–3215. https://doi.org/10.1021/ac00127a063.
- (60) Pawliszyn, J. Chemical Sensing Using Concentration Gradient Transients Produced during Diffusive Transport of Analytes. *Anal Chem* **1992**, *64* (14), 1552–1555. https://doi.org/10.1021/ac00038a010.
- (61) Palagi, S.; Fischer, P. Bioinspired Microrobots. Nat Rev Mater 2018, 3 (6), 113–124. https://doi.org/10.1038/s41578-018-0016-9.
- (62) Plutnar, J.; Pumera, M. Chemotactic Micro- and Nanodevices. *Angewandte Chemie International Edition* **2019**, *58* (8), 2190–2196. https://doi.org/10.1002/ANIE.201809101.
- (63) Yang, Z.; Abbott, N. L. Spontaneous Formation of Water Droplets at Oil-Solid Interfaces. *Langmuir* **2010**, *26* (17), 13797–13804. https://doi.org/10.1021/la101740p.
- (64) Kamenka, N.; Lindman, B.; Brun, B. Translational Motion and Association in Aqueous Sodium Dodecyl Sulphate Solutions. *Colloid and Polymer Science Kolloid-Zeitschrift & Zeitschrift für Polymere* **1974**, *252* (2), 144–152. https://doi.org/10.1007/BF01555539.
- (65) Marbach, S.; Yoshida, H.; Bocquet, L. Osmotic and Diffusio-Osmotic Flow Generation at High Solute Concentration. I. Mechanical Approaches. *Journal of Chemical Physics* **2017**, *146* (19). https://doi.org/10.1063/1.4982221.
- (66) Yoshida, H.; Marbach, S.; Bocquet, L. Osmotic and Diffusio-Osmotic Flow Generation at High Solute Concentration. II. Molecular Dynamics Simulations. *Journal of Chemical Physics* **2017**, *146* (19). https://doi.org/10.1063/1.4981794.

- (67) Lee, C.; Cottin-Bizonne, C.; Biance, A. L.; Joseph, P.; Bocquet, L.; Ybert, C. Osmotic Flow through Fully Permeable Nanochannels. *Phys Rev Lett* **2014**, *112* (24), 1–5. https://doi.org/10.1103/PhysRevLett.112.244501.
- (68) Stone, H. A. A Simple Derivation of the Time-Dependent Convective-Diffusion Equation for Surfactant Transport along a Deforming Interface. **2018**, *111* (1990), 5–7. https://doi.org/10.1063/1.857686.
- (69) Yesil, F.; Suwa, M.; Tsukahara, S. Anchoring Energy Measurements at the Aqueous Phase/Liquid Crystal Interface with Cationic Surfactants Using Magnetic Fréedericksz Transition. *Langmuir* **2018**, *34* (1), 81–87. https://doi.org/10.1021/acs.langmuir.7b03005.
- (70) Oshkai, P.; Geveci, M.; Rockwell, D.; Pollack, M. Imaging of Acoustically Coupled Oscillations Due to Flow Past a Shallow Cavity: Effect of Cavity Length Scale. *J Fluids Struct* **2005**, *20* (2), 277–308. https://doi.org/10.1016/j.jfluidstructs.2004.10.010.
- (71) Palharini, R. C.; Scanlon, T. J.; White, C. Chemically Reacting Hypersonic Flows over 3D Cavities: Flowfield Structure Characterisation. **2018**, *165*, 173–187. https://doi.org/10.1016/j.compfluid.2018.01.029.
- (72) Chang, C. H.; Franses, E. I. Modified Langmuir-Hinselwood Kinetics for Dynamic Adsorption of Surfactants at the Air/Water Interface. *Colloids and Surfaces* **1992**, *69* (2–3), 189–201. https://doi.org/10.1016/0166-6622(92)80230-Y.
- (73) Peaudecerf, F. J.; Landel, J. R.; Goldstein, R. E.; Luzzatto-Fegiz, P. Traces of Surfactants Can Severely Limit the Drag Reduction of Superhydrophobic Surfaces. *Proc Natl Acad Sci U S A* **2017**, *114* (28), 7254–7259. https://doi.org/10.1073/pnas.1702469114.
- (74) Ghosh, P. Coalescence of Air Bubbles at Air-Water Interface. *Chemical Engineering Research and Design* **2004**, *82* (7), 849–854. https://doi.org/10.1205/0263876041596715.
- (75) Patrício, P.; Leal, C. R.; Pinto, L. F. V.; Boto, A.; Cidade, M. T. Electro-Rheology Study of a Series of Liquid Crystal Cyanobiphenyls: Experimental and Theoretical Treatment. *Liq Cryst* **2012**, *39* (1), 25–37. https://doi.org/10.1080/02678292.2011.610471.
- (76) Wang, X.; Miller, D. S.; De Pablo, J. J.; Abbott, N. L. Organized Assemblies of Colloids Formed at the Poles of Micrometer-Sized Droplets of Liquid Crystal. *Soft Matter* **2014**, *10* (44), 8821–8828. https://doi.org/10.1039/c4sm01784f.

